

pubs.acs.org/molecularpharmaceutics Article

Disparities of Single-Particle Growth Rates in Buried Versus Exposed Ritonavir Crystals within Amorphous Solid Dispersions

Scott R. Griffin, Nita Takanti, Sreya Sarkar, Zhengtian Song, Andrew D. Vogt, Gerald D. Danzer, and Garth J. Simpson*



Cite This: Mol. Pharmaceutics 2020, 17, 4564-4571

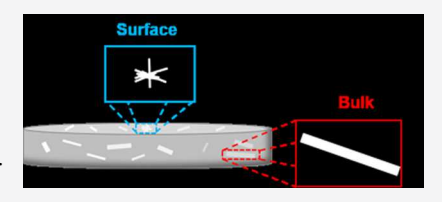


ACCESS

III Metrics & More

Article Recommendations

ABSTRACT: Seeded growth rates of ritonavir in copovidone at 75% relative humidity (RH) and 50 °C were evaluated by single-particle tracking second harmonic generation (SHG) microscopy and found to be ∼3-fold slower for crystallites at the surface compared to the bulk. The shelf lives of final dosage forms containing amorphous solid dispersions (ASDs) are often dictated by the rates of active pharmaceutical ingredient crystallization. Upon exposure to elevated RH, the higher anticipated water content near the surfaces of ASDs has the potential to substantially impact nucleation and growth kinetics relative to



the bulk. However, quantitative assessment of these differences in growth rates is complicated by challenges associated with discrimination of the two contributions (supersaturation and molecular mobility) in ensemble-averaged measurements. In the present study, "sandwich" materials were prepared, in which sparse populations of ritonavir single-crystalline seeds were pressed between two similar ASD films to assess bulk crystallization rates. These sandwich materials were compared and contrasted with analogously prepared "open-faced" samples, without the capping film, to assess the surface crystallization rates. Single-particle analysis by SHG microscopy time-series during in situ crystallization produced average growth rates of 3.8 μ m/h for bulk columnar crystals with a particle-to-particle standard deviation of 0.9 μ m/h. In addition, columnar crystal growth rates for surface particles were measured to be 1.3 μ m/h and radiating crystal growth rates for surface particles were measured to be 1.0 μ m/h, both with a particle-to-particle deviation of 0.4 μ m/h. The observed appearance of radiating crystals upon surface seeding is attributed to reduced ritonavir solubility upon water adsorption at the interface, leading to higher defect densities in crystal growth. Despite substantial differences in crystal habit, correction of the surface growth rates by a factor of 4 from geometric effects resulted in relatively minor but statistically significant differences in the growth kinetics for the two local environments. These results are consistent, with viscosity being a relatively weak function of water absorption coupled with primarily diffusion-limited growth kinetics.

KEYWORDS: second harmonic generation, active pharmaceutical ingredients, amorphous solid dispersions, nonlinear optics, crystallization kinetics

■ INTRODUCTION

Solid-state forms of active pharmaceutical ingredients (APIs) significantly affect the oral bioavailability in the final dosage form because of low aqueous solubility. 1,2 Amorphous solid dispersions (ASDs) have been used to increase the bioavailability of low-solubility APIs by casting the API in an amorphous glassy polymer matrix to prevent crystallization at supersaturated states. Intimate mixing in a glassy state with the pharmaceutically appropriate excipients traps the API kinetically in an amorphous form, which is typically a metastable state with increased apparent solubility, free energy, and dissolution rate.^{3,4} However, the primary challenge is assuring long-term physical stability in the amorphous state as the amorphous forms have increased chemical and thermodynamic activities compared to crystalline analogues. Although the amorphous API has increased bioavailability and greater oral absorption, amorphous forms of the API also have greater chemical and physical instability. This instability of amorphous solids leads to crystal growth and crystal nucleation within the API. Crystal formation of the API negatively influences the bioavailability and stability and consequently decreases the shelf life of the drug. ^{1,3} Measurements capable of informing observed crystal growth at the early stages of formation at conditions of ASD storage can reduce the overall timeframe required for evaluating stability, both at the surface of the ASD film and in the ASD bulk. ¹

There are many models that have described the mechanism of crystal growth on the surface of APIs in ASDs in the last 10 years, with comparisons to crystal growth in the bulk. $^{5-10}$ One

Received: July 17, 2020
Revised: October 16, 2020
Accepted: October 19, 2020
Published: November 5, 2020





is the tension-release model: Since the density of crystals is higher than that of amorphous glass, the stress and strain effects in the bulk are much stronger than at the surface, which causes faster crystal nucleation and growth on the surface.⁶ However, Tanaka argues that crystal formation in a glassy material induces stress around the crystal, leading to a volume contraction upon the crystal. As the volume of glassy material surrounding the crystal increases relative to the volume of the crystal, there is an increase in mobility, leading to further crystallization. Based on this theory, crystal growth on surfaces will be slower than in the bulk, as there is significantly more glassy material surrounding crystals in the bulk than on the surface. Another well-known model is the surface mobility model: The higher crystal growth rate on the surface is due to higher mobility of surface molecules.^{8,9} In addition, the higher mobility of surface molecules also results in a faster nucleation rate. The third model is based on the effects of molecular packing on the surface versus in the bulk. 10 Further complicating the modeling of mechanisms of crystal growth, additives can profoundly impact crystallization kinetics, the effects of which have the potential to be distinctly different for surface versus bulk crystallization. 11 Diffusion-limited models for crystal growth kinetics in the presence of additives do not adequately capture the observed trends in the literature, with significant increases in surface crystallization rates routinely reported in amorphous molecular glasses. 12,13 Additional measurement tools capable of sensitive and independent interrogation of surface and bulk crystal growth kinetics and mechanisms may help address lingering ambiguities between these two growth conditions.

A diverse suite of tools routinely used for accelerated stability testing of APIs in ASDs has the potential to help address the mechanisms driving surface and bulk crystal formation. However, most accelerated stability tests are performed by using powdered pharmaceutical samples, which only provide average information of the entire sample and makes it difficult to reveal API crystallization at different locations. API crystallization kinetics in the bulk have shown to be different from that on the surface. For example, Zhu, et al. demonstrated that crystal growth rate at the surface of pure amorphous griseofulvin is 10- to 100-fold faster than that in the bulk. Zhu attributed the difference to the fact that the surface crystallization rate was much less temperature-dependent than the bulk under the glass transition temperature because of uniformity in particle size distribution on the surface. 13 In addition, Yu et al. reported differences in surface and bulk crystallization rates for amorphous nifedipine (NIF) melted with small relative concentrations of polyvinylpyrrolidone (PVP) of different molecular weights to make a twocomponent amorphous system. 12 The authors reported strong inhibition of crystallization in the bulk from PVP, with a much weaker effect observed for surface crystallization rates. Many explanations were considered to explain the differences in crystallization kinetics, such as PVP concentration being lower at the surface than in the bulk, and the hypothesized higher mobility at the surface resulting in a reduced inhibitory impact of PVP on crystal growth. 12 As the difference in crystallization for bulk versus surface of the drug is still poorly understood, there is a need for further studies to understand the crystal growth distribution within the final dosage form of the amorphous API. Accelerated stability testing of crystal growth for bulk versus surface can lead to a better assessment of the spatial heterogeneity of stability of the ASDs as well as its

bioavailability.^{2,12} Most notably, these previous studies were performed either with purely or predominantly API, which may not be representative of behaviors arising in ASDs, in which the API is typically the minority species.

Several analytical techniques are commonly used for accelerated stability testing that can potentially be brought to bear for surface versus bulk analysis, including polarized light microscopy (PLM), powder X-ray diffraction (PXRD), Raman spectroscopy, IR spectroscopy, solid-state NMR spectroscopy, and so forth. Even though PLM has been used to detect crystallinity and determine crystal nucleation rates, 14 the spatial resolution is hindered by diffraction limitation. 15,16 Although PXRD is hailed as the "gold standard" to identify the solid form and degree of crystallinity of the API, the technique typically requires the sample to have appropriate particle size, orientation, and thickness. In addition, PXRD obtains broader reflections and lower absolute intensities for smaller average crystallite size and for decreased crystal quality. 16,17 Although spectroscopic methods, such as IR^{18,19} and Raman, ^{19,20} can obtain raw material crystalline and polymorph identification in a non-destructive manner, these methods are more conducive to investigate crystallinity on the surface, with little studies have being done in the bulk. For example, although Bhatia et al. were able to use high-resolution low-frequency Raman in order to analyze the crystal structure on the surface for both amorphous and crystalline films of molybdenum trioxide, Raman was unable to analyze the bulk nanocrystal structure without implementation of XRD as well.²¹ In addition, even though the new spectroscopic improvements concerning ssNMR improved sensitivity in order to give unique insights into the microscopic and macroscopic structure of APIs, these studies have been mainly applied to microcrystalline solids from ground commercial tablets, leading to average ensemble measurements.²² Similar to the techniques discussed, most other benchtop methods do not have great penetration or high enough sensitivity to measure trace crystallinity within a bulk sample. Thakral et al. used synchrotron X-ray diffractometry to quantify crystallization from the surface to core of a tablet, which enabled investigation of heterogeneous crystallization in a tablet.²³ More recently, Berzins and Suryanarayanan used synchrotron X-ray diffractometry in order to detect differences in crystallization on the surface and crystallization in the bulk and non-nucleated surfaces using the broadening of the crystallization exotherm for compressed tablets of amorphous sucrose and sucrose-PVP.²⁴ However, X-ray diffraction patterns cannot provide information to assess nucleation and crystal growth kinetics. Furthermore, access to a synchrotron X-ray light source is not commonly available for pharmaceutical formulation development. Overall, these techniques obtain ensemble-average measurements, which lose microscopic information such as crystal nucleation rates and kinetic growth rates, and do not have sensitive detection of crystallinity deep within tablets and powders. 1,2

Recently, nonlinear optical microscopy has emerged with potential as an analytical tool for quantitative analysis of trace crystallinity within pharmaceutical materials. Nonlinear optical microscopy has been used to probe initial stages of crystal formation as it provides an advantage for pharmaceutical research with temporal sensitivity, spatial selectivity due to non-destructive nonlinear excitation, and increased imaging speed for dynamic processes. 1,25,26 Nonlinear optical measurements enable the recovery of crystal growth rates within powders or thin films that have $\leq 1\%$ crystallinity. 1,2,27

Specifically, second harmonic generation (SHG) is an application of nonlinear optics that results in the frequency doubling of light upon interaction of non-centrosymmetric crystals, where the interactions of the photons lead to resonant enhancement.^{2,26} SHG is able to quantify API crystallization with detection limits in the parts per million regime in comparison with competing techniques that have detection limits around ~10% crystallinity. 25 The primary advantage of SHG is the increase in signal-to-noise. When using SHG, there is a suppression of the background since the disordered, amorphous material of the ASD does not produce a coherent signal. The higher signal-to-noise leads to a chemically selective visualization of the crystallites in the complex mixed system as opposed to other techniques that do not provide this clear visualization. 1,26,28 With the improvement in signal-tonoise, SHG allows for dynamic processes, such as crystallization, to be followed in real time. Therefore, quantitative determination of crystal nucleation, growth kinetics, and macroscopic crystallization rates from a single set of measurements can be obtained with improvement in lower limits of detection and greater linear dynamic range. Podzemná et al. were able to demonstrate real-time imaging when measuring crystal growth kinetics and nucleation kinetic rates of germanium disulfide.²⁹ Overall, SHG would serve as a sensitive and selective tool for detection and characterization of both surface and bulk materials.1

In this work, SHG microscopy was performed within the bulk and at the surface of seeded ritonavir crystals in copovidone for high-contrast quantitative analysis of crystallization kinetics. As SHG is highly selective for crystals of homochiral molecules, quantitative analysis of crystal growth on a per-particle basis can be obtained. As such, growth rates were independently determined from the "time-lapsed" image analysis over 48 h for individual crystals. A controlled environment for in situ stability testing (CEiST) chamber with 10 sample wells was used, which allowed for continuous monitoring of the individual crystal over 48 h under 50 °C and 75% relative humidity (RH), typical of previous ASD analysis. As the sensitive and non-destructive SHG microscopy continuously monitored the samples in CEiST in the same fields of view (FoVs) over time, the signal-to-noise of crystal growth rate was significantly improved with a lower number of samples.³⁰ Differences observed in growth rate kinetics from surfaces versus the bulk were interpreted in terms of supersaturation and molecular mobility.

■ METHODS

ASD samples of ritonavir (15%), sorbitan monolaurate (10%), copovidone (74%), and colloidal silicon dioxide (1%) were prepared as hot melt extrudates. The extrudates were made using a lab scale Thermo Scientific Process 11 Hygienic Parallel twin-screw extruder fed gravimetrically at 0.750 kg/h with a screw speed of 250 rpm. Temperatures in the heating zones ranged from 15 to 150 °C. The extrudates were milled using a Fitzmill L1A at 6000 rpm and a screen size of 0.033 inches, round hole. Samples without the sorbitan monolaurate were also made, in which the copovidone weight percent was increased to 84%.

The Specac Atlas Constant Thickness Film Maker Accessory was implemented in order to make thin films of these ASD powders, which would be used to prepare samples with seeded crystals on the surface. A sample of 50–60 mg of the ASD was centered and dispersed between two pieces of an aluminum

foil, which were previously cut with PunchBunch SlimLock Medium Punch—circle 1 in. radius. The Film Maker Accessory was then set to a temperature of 115 °C using a 100 μ m spacer. After the sample was heated up for 5 min, the Film Maker Accessory was then put under a pressure of 4 tons per 3 in.². After 10 min under pressure, the temperature on the Film Maker Accessary was decreased to 65 °C, while the pressure was maintained at 4 tons. After the Film Maker Accessary reached 65 °C, the pressure was released, and the film was removed from the apparatus and aluminum foil and set aside to cool, creating a single thin ASD film. Using a microscope, single crystals were manually placed onto the film.

The thin films containing the seeded crystals could undergo further sample preparation in order to obtain samples that represented seeded crystals in the bulk. The surface films with seeded crystals were placed back into the Film Maker Accessory, and a film without seeded crystals was placed on top, depicting a "sandwich" (film-crystal-film), in which the "sandwich" was again placed between two pieces of the aluminum foil. The Film Maker Accessory was set to 98 °C with a 250 μ m spacer and pressurized to 1.25 tons per 3 in.². As with a single thin film, the temperature and pressure remained constant for 10 min, following which time the temperature was reduced to 65 °C. After the Film Maker Accessary reached 65 °C, the film was removed from the apparatus and the aluminum foil, creating a film that contained seeded crystals in the bulk ASD. For both surface and bulk seeded preparations, the thin films were carefully cut and placed into the CEiST. Information on the CEiST's design is described in more detail in previous work.³⁰

Accelerated stability testing was performed using a SONICC (second order for nonlinear imaging for chiral crystals) microscope from Formulatrix (Bedford, MA) for SHG imaging. The SONICC microscope was modified in-house such that the sample holder was switched for a 3D printed holder modified to mount the CEiST. The RH was held at 75% and the temperature kept at 50 °C within the CEiST chamber throughout the duration of the experiment. Samples were then imaged over a course of 48 h, with data being collected every hour in the same FoV for each well using 200 mW excitation power with an exposure time of 447 ms for every hour. In the first 2 h, data were also collected using 350 mW excitation power with an exposure time of 894 ms for the first 2 h.

Data analysis was primarily done using FIJI (FIJI Is Just ImageJ). Single crystals were manually tracked through the 48 images (one image collected for every hour the experiment ran), and the area and perimeter of each monitored crystal were obtained through the plug-in features of FIJI. Using these two known parameters and the equations for area and perimeter, the length was calculated. For columnar crystals, the length of the crystal was then plotted over the course of 48 h for 20 bulk crystals and 20 single surface crystals. In addition, the length for 20 radiating crystals was calculated by assuming a circular area and by relating the single-particle growth rate to the fast axis growth along the diameter. Solving for the diameter from the area provided the length and subsequent growth rates for the radially growing crystals.

■ RESULTS AND DISCUSSION

SONICC and the CEiST multiwell chamber were used to determine the growth rates of individual ritonavir crystals seeded onto "open-faced" and "sandwiched" samples. Figure 1

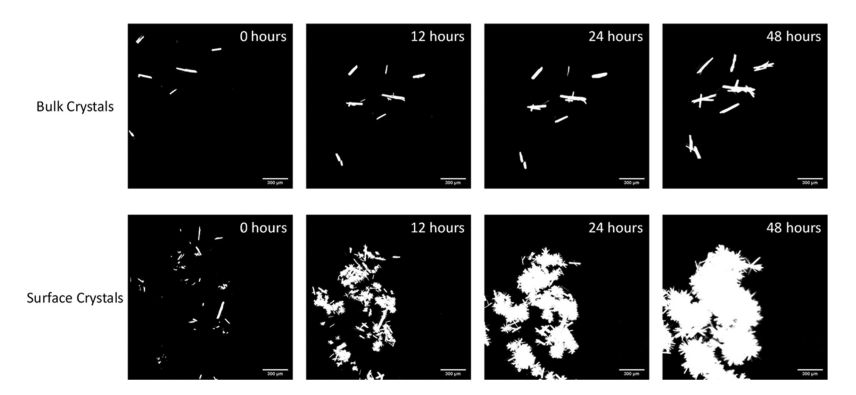


Figure 1. SHG images over time of seeded crystals pressed between two ASD films (bulk) and of seeded crystals on top of the pressed film (surface).

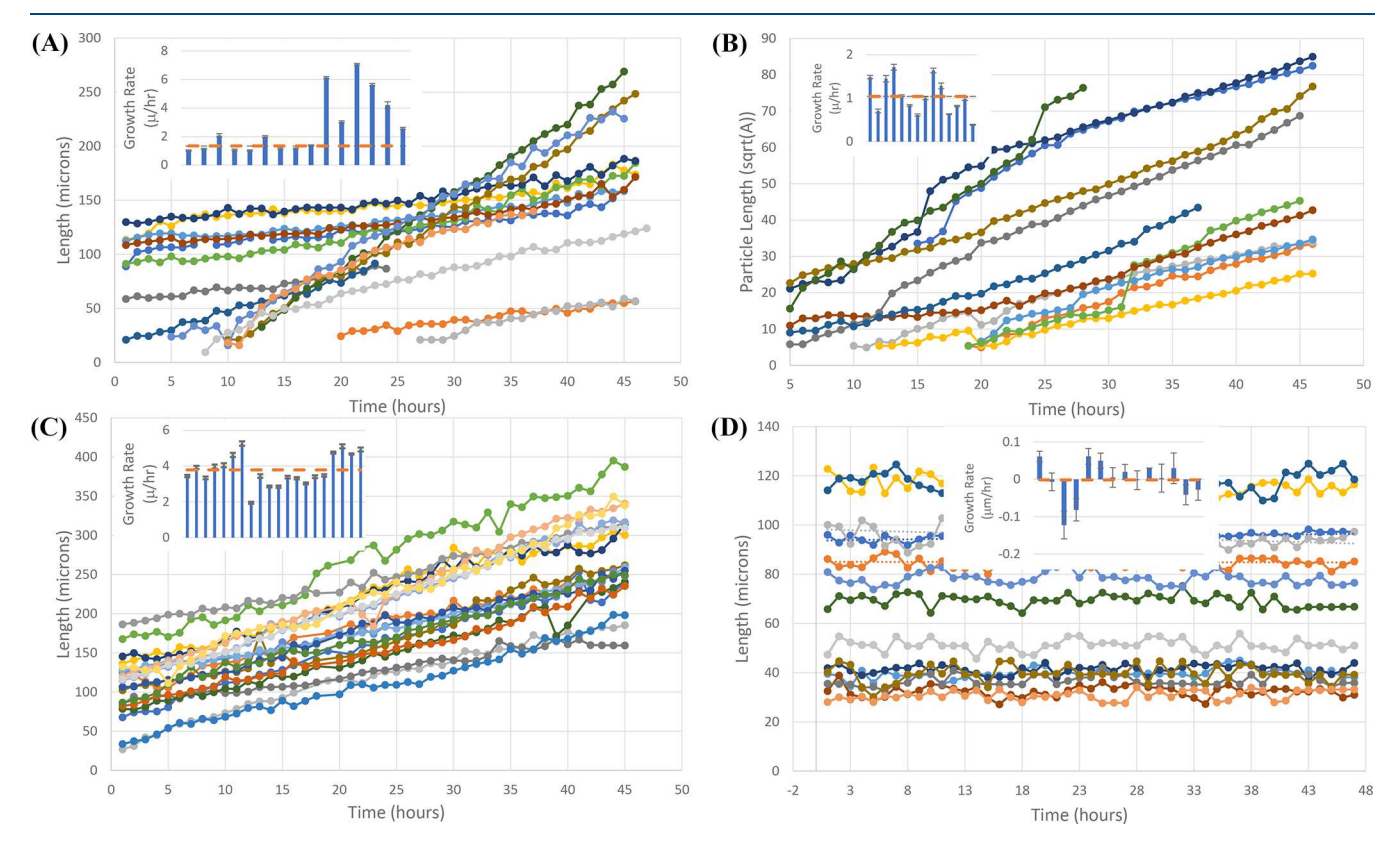


Figure 2. Individual crystal growth distributions for (A) single crystals on the surface, (B) radiating crystals on the surface, (C) single crystals in bulk, and (D) single crystals in a low RH environment. Each plot has 14 or more different crystals selected from different FoVs, and the inset in each plot shows the crystal growth rate distributions with the average shown as a dashed line. In (A), the average growth rate reported includes the slower growing particles, only to enable a direct comparison with the other crystal growth rates reported that share the same crystal form.

shows an example of crystal growth on the open-faced samples and sandwiched samples over a 48 h time period. Crystal growth can be seen primarily along the long axis of the rodlike crystals in both cases. However, crystals in open-faced samples show a radial growth habit, while sandwiched crystals show a columnar growth habit. The apparent increase in crystallinity measured by volume for surface-seeded crystal growth in Figure 1 is largely a consequence of the higher volume occupied by radial growth relative to single-crystal columnar growth.

This difference in crystal habit is tentatively attributed to a higher water content and/or surfactant at the ASD surface relative to the bulk. Ritonavir is well-known to exhibit low aqueous solubility, suggesting that water adsorption or absorption at high RH would likely increase the supersaturation of ritonavir adjacent to the film surface. The amorphous API is kinetically prevented from adopting a low-energy crystalline form, increasing the Gibbs free energy and generally leading to thermodynamically metastable assemblies. During storage, water acts as a potent plasticizer and can decrease the $T_{\rm g}$ of the amorphous solid upon absorption. This decrease in $T_{\rm g}$ can increase the molecular mobility and kinetically promote transitioning to low-energy crystalline states. Tocal increases in surface supersaturation promote nucleation of crystal defects. Subsequent growth from a polycrystalline source can produce radial growth habits similar to those observed. This phenomenon of increasing nucleation/defect propagation leads to an increase in total

crystallinity of the sample at the surface versus within the bulk as a consequence of radial versus columnar growth habits, respectively. The authors hypothesize that the newly nucleated particles are ritonavir crystal form I (as opposed to the seeded crystal form II), which has been shown in previous work to grow faster and spontaneously nucleate. The primary mechanism for crystal growth for ritonavir is dependent on hydrogen bond formation (new or exchanged); form I has a greater percentage of surface area with exposed hydrogen bond donors and acceptors than form II, leading to faster bulk crystallization and dissolution rates. In addition, primary nucleation from a solution of ritonavir would favor the crystal form whose structure is closest in energy and arrangement to molecules in solution, which is typically form I. 36

Single-particle growth distributions are shown in Figure 2 along with uncertainties in the parameters recovered from linear fitting of the growth curves. For both the bulk and surface regions, the particle-to-particle deviation exceeds the errors of the fits, suggesting statistically significant differences. In the bulk, relatively minor differences in growth rates were observed, similar in magnitude to those reported previously, and attributed to subtle differences in the local environments within the glassy matrix. In contrast, the differences in the growth rates of individual particles seeded on the surface exhibit clear evidence (Figure 2A) of a bimodal distribution. Most of the crystals measured grow slowly $(1.3 \pm 0.4 \,\mu\text{m/h})$, while a few grow at a significantly faster rate $(4.8 \pm 1.8 \,\mu\text{m/h})$. The faster growing particles tend to nucleate during the experiments rather than emerging from obvious seed crystals.

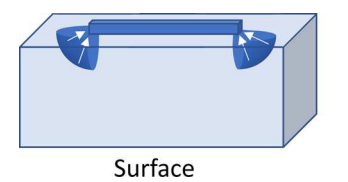
Additional tests, for the same FoVs, of the measured aspect ratio were performed to determine whether the slow- and fastgrowing particles on the surface were statistically significantly different. The mean of the measured aspect ratios was 4.7 \pm 1.5 for the slow particles and 8.8 ± 2.6 for the fast particles. The first of these two aspect ratios is statistically indistinguishable from the analogous measurements for the bulk seeded crystals. However, the fast-growing particles nucleated during the experiment were statistically distinct from both the slow surface particles and bulk particles within a confidence of 90%. These collective observables are consistent with the fastgrowing particles arising from a crystal form unique from the crystal seeds used for surface versus bulk growth rate analysis. Additional measurements specific to single-particle crystal form such as synchrotron XRD or localized Raman analysis are beyond the scope of the present study, such that this hypothesis is tentative.^{37–39} In any case, these outlying crystal forms were excluded from subsequent analysis of the differences in growth kinetics. It is worth noting the importance of single-particle growth rate analysis in order to enable this assessment; ensemble-averaged results would otherwise produce bias in the growth rates measured from crystals at the surface, if the individual outlying particles were

Interestingly, individual single-crystal growth rates are notably higher in the bulk than the growth rates on the surface. This result is highlighted in Figure 2. The crystal growth rates for crystals within the bulk material were roughly 3 times those of crystals on the surface. The average crystal growth rate within the bulk was $3.8 \pm 0.9 \ \mu \text{m/h}$, while the average growth rate on the surface was $1.3 \pm 0.4 \ \mu \text{m/h}$.

Several possible explanations for the disparity in surface versus bulk growth rates were considered, including spatial differences in water content. Under diffusion-limited conditions, a gradient in water content could arise within the polymer matrix, with higher water content closer to the surface of the ASD film. If the higher water content correlates with slower diffusion within the polymer, bulk growth rates at lower water contents would be expected to exhibit slower crystal growth rates. However, studies of ASD materials showed that higher water absorption was observed to decrease the viscosity and increase the mobility in the amorphous state with different polymer additives. 40,41 In addition, a control experiment was performed to assess the impact of water content (Figure 2D) in which the CEiST chamber was brought to 50 °C and 0% RH by the use of a desiccant. Crystals seeded and maintained at low RH showed no significant growth on the surface or within the bulk. As a consequence of this experiment, we concluded that increases in water content through absorption within the ASD are likely to correlate with increases in crystal growth rate. Increased water content adjacent to the interface would contribute to lower viscosity and faster diffusion, such that surface growth would be significantly faster at the surface than in the bulk rather than slower as observed experimentally. Consequently, we concluded that the samples likely exhibited similar water content throughout the ASDs, given the relatively small, but statistically significant, differences in growth rates both at the surface and in the bulk with elevated RH.

Similar arguments were considered for possible gradients in composition arising from surface partitioning of the surfactant. Surface partitioning could impact API mobility to and across the interface and crystal growth kinetics. Previous studies have shown that surfactant layers can impact API mobility. In studies of theophylline with lung surfactants, agglomeration of the API within the surfactant layer resulted in crystal nucleation and reduced molecular transport through the lung surfactant layer. 42 In other work, the presence of a surfactant was found to affect the crystal form produced upon crystallization of glutamic acid. 43 In the present study, the kinetics is consistent with diffusion-limited crystal growth, such that the growth rates are unlikely to be substantially affected by subtle free-energy differences at the interfaces because of the presence of monomolecular surfactant layers at the interfaces. In previous studies of similarly prepared materials, the addition of a surfactant resulted in substantial increases in crystal growth kinetics attributed to a reduction in viscosity relative to surfactant-free ASDs. 30 Based on these results, one would expect an increase in the surfactant concentration adjacent to the interface to result in lower viscosity and higher API mobility, in direct opposition to the trends observed experimentally. Therefore, we conclude that surface partitioning of surfactant to the tablet and/or crystal interfaces is unlikely to explain the observation of lower growth rates for crystals positioned at the ASD surface. However, differences in interfacial free energy associated with surfactants may provide a potential explanation for the radial crystal growth appearing from seeding with single crystals at the interface as well as the apparent nucleation of a second crystal form at the surface.⁴³

Possible differences in surface and bulk growth rates were also considered from geometric effects related to molecular diffusion, as illustrated in Figure 3. For "sandwiched" crystals under diffusion-limited conditions, a concentration gradient forms in the region immediately adjacent to the growth planes, with the degree of supersaturation lowering closer to the interface. Contours of constant API concentration arising in the medium adjacent to the growth plane will be approximately described by hemispherical surfaces, the net flux through which



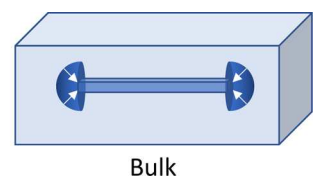


Figure 3. Illustration of the geometric effects on diffusion-limited crystal growth on the surface and in the bulk.

dictates crystal steady-state growth rate. The area of this isosurface is estimated by integration over a solid angle corresponding to a hemisphere, given by $A = \int_{\pi}^{-\pi} \int_{\pi/2}^{0} \sin \theta \, d\theta \, d\phi$ in spherical coordinates, in which θ is the polar tilt angle along the growth plane normal and ϕ is the azimuthal angle. In contrast, the "open-faced" crystals seeded on the ASD surface only have access to an influx from just the lower half of the hemispherical surface in intimate contact with the ASD film (corresponding to the limits in ϕ evaluated from 0 to π instead of $-\pi$ to π). Since the flux to the growth plane is reduced by a factor of 2 in comparison to bulk crystals, a growth rate correction factor of 2:1 (bulk/surface) is expected for diffusion-limited growth at each growth plane, corresponding to a 2:1 total expected difference in growth rates. 44

The disparity in growth rate found in this study was \sim 3:1 (bulk/surface), which is in reasonably good qualitative agreement with the 2:1 reduction in surface growth expected from geometric considerations of diffusion-limited growth.

Several mechanisms were considered for the origin of the disparit between the 2:1 geometric effect and the experimentally observed ~3:1 difference in growth rates. Both the water content and the presence of surfactants can significantly impact the crystal growth rates within ASDs as reported previously. ^{31–33,42} Copovidone is known to exhibit significant water absorption at high humidities such as those used in the experiments performed herein. 45 For crystals seeded within the bulk, onset of crystal growth arose within ~ 1 h, consistent with relatively fast water permeation throughout the copovidone films (<1 h). Since the water content is expected to be similar throughout the copovidone-based matrix, the ritonavir diffusion rate adjacent to the interface to facilitate crystal growth is reasonably expected to be similar to that within more deeply buried bulk regions. However, at the interface itself, surfactants have been found to either increase or decrease crystal growth rates depending on the API and surfactant molecule interactions. 42,46 Surfactants have been shown to increase crystal growth rates by increasing the molecular diffusion of the API molecule within the thin interfacial layer. 46 Conversely, the surfactant partitioning to the interface can result in a blocking layer inhibiting the diffusion of the API molecules to the growth plane. The surfactants can also adsorb to the surface of crystal growth planes themselves, which can further inhibit the kinetics of crystal growth depending on the surfactant/API molecule interactions. 46 These two effects together provide a possible origin for the relatively subtle but statistically significant decrease in the expected growth rate differences from the geometric model considering only bulk diffusion-limited growth.

The observations reported herein indicate slower growth kinetics at ASD surfaces relative to the bulk predominantly driven by geometric effects and is juxtaposed to numerous previous studies in the literature demonstrating enhanced crystal growth rates for APIs at surfaces relative to analogous

bulk. For example, studies of amorphous griseofulvin 13 and amorphous NIF doped with small quantities (1-5%) of organic polymer PVP¹² exhibited faster surface growth relative to analogous bulk values. The notable difference in observed behaviors may arise from the disparity in mass fraction of API in the ASD. The present studies were performed with only 15% API entrained within a glassy matrix, while previous studies characterized trends in materials with >95% API. These two different composition regimes may result in major differences in interactions driving crystal growth kinetics (e.g., molecular diffusion, internal energy barriers, heat dissipation, etc.). The previous studies with low doping are not representative of practical ASDs used in final dosage forms as API loadings in the polymer matrix can approach 30-40%. 47 As such, the bulk-to-surface 4-fold growth rate difference observed in this study with 15% API is more representative of the kinetics expected in ASDs similar to those currently integrated into commercial final dosage forms.

CONCLUSIONS

We demonstrate single-particle tracking in a CEiST chamber using SHG microscopy to monitor crystal growth kinetics within bulk material and on the surface of ASDs. In the ritonavir/copovidone system explored, bulk crystal growth rates were found to be ~3-fold greater than similarly prepared seeded crystals placed at the ASD film surface. The reduction in growth rate at the surface is primarily attributed to geometric effects under diffusion-limited growth conditions where surface particles are expected to grow slower due to diffusion from less material overall. Nevertheless, the radial surface crystal growth habit led to higher total crystallinity than in the bulk, which exhibited exclusively columnar growth. Single-particle tracking also enabled isolation of a second population of surface crystals exhibiting faster growth rates and higher aspect ratios than the seeded crystals. The collective results highlight the advantages of single-particle tracking enabled by SHG microscopy of ASD materials; integration over all of the individual particles masks the detail of disparities arising within the crystal populations depending on the timing and location of crystal formation. Recovery of single-particle information provides information for improving the modeling and simulation of crystal growth rates and particle size distributions within ASD materials expected during storage and handling.

As one interesting example, increasing the surface areas of ASD particles within a formulation could lead to either fast or slow crystal growth, depending on the interplay between a geometric effect slowing growth and differences in crystal habit and/or crystal form that could encourage increases in overall crystallinity. Improved understanding/modeling of the local differences in the API concentration and diffusion arising at the surface and within the bulk can lead to informed decision-making in designing formulations. Assuming other ASDs exhibit qualitatively similar richness in particle-to-particle behaviors, SHG-enabled particle tracking in controlled environmental conditions may provide a broadly utilitarian framework for rational optimization of particulate conditions when preparing final dosage forms incorporating milled ASDs.

Although beyond the scope of the present study, future work is aimed at creating a higher throughput version of the CEiST method capable of simultaneously tracking growth trends versus temperature and humidity. Along with a temperature gradient throughout the high throughput platform, different

RH conditions will also be evaluated. The temperature and RH array platform will allow for analysis of trends of crystal growth due to varied RH and will provide basis for control experiments for this work.

AUTHOR INFORMATION

Corresponding Author

Garth J. Simpson — Department of Chemistry, Purdue University, West Lafayette, Indiana 47907, United States; orcid.org/0000-0002-3932-848X; Email: gsimpson@purdue.edu

Authors

Scott R. Griffin – Department of Chemistry, Purdue University, West Lafayette, Indiana 47907, United States Nita Takanti – Department of Chemistry, Purdue University, West Lafayette, Indiana 47907, United States

Sreya Sarkar – Department of Chemistry, Purdue University, West Lafayette, Indiana 47907, United States

Zhengtian Song — Department of Chemistry, Purdue University, West Lafayette, Indiana 47907, United States Andrew D. Vogt — AbbVie Inc., North Chicago, Illinois 60064, United States

Gerald D. Danzer – AbbVie Inc., North Chicago, Illinois 60064, United States

Complete contact information is available at: https://pubs.acs.org/10.1021/acs.molpharmaceut.0c00744

Notes

The authors declare the following competing financial interest(s): Andrew D. Vogt and Gerald D. Danzer are employees of AbbVie and may own AbbVie stock. AbbVie helped sponsor and fund the study; contributed to the design; participated in the collection, analysis, and interpretation of data, and in writing, reviewing, and approval of the final publication. The other authors declare no conflicts of interest related to this work.

ACKNOWLEDGMENTS

The authors gratefully acknowledge funding for the present work from the National Science Foundation through an NSF-GOALI award-1710475 and the U.S. Department of Education through the pharmaceutical engineering 2015 GAANN award-P200A150136. In addition, S.S., Z.S., S.R.G., and G.J.S. acknowledge financial support from AbbVie. S.S. also acknowledges support from an NSF research supplement award-1643745. The authors would also like to acknowledge Formulatrix for the use of SONICC instrumentation, Dr. Hartmut Hedderich, Randy Replogle, and Casey J. Smith for their assistance in design and construction of the CEiST platform, and Alex Ruggles from AbbVie for the samples used in these studies.

■ REFERENCES

- (1) Kissick, D. J.; Wanapun, D.; Simpson, G. J. Second-Order Nonlinear Optical Imaging of Chiral Crystals. *Annu. Rev. Anal. Chem.* **2011**, *4*, 419–437.
- (2) Schmitt, P. D.; DeWalt, E. L.; Dow, X. Y.; Simpson, G. J. Rapid Discrimination of Polymorphic Crystal Forms by Nonlinear Optical Stokes Ellipsometric Microscopy. *Anal. Chem.* **2016**, *88*, 5760–5768.
- (3) Ivanisevic, I. Physical Stability Studies of Miscible Amorphous Solid Dispersions. *J. Pharm. Sci.* **2010**, *99*, 4005–4012.

- (4) Kennedy, M.; Hu, J.; Gao, P.; Li, L.; Ali-Reynolds, A.; Chal, B.; Gupta, V.; Ma, C.; Mahajan, N.; Akrami, A.; Surapaneni, S. Enhanced Bioavailability of a Poorly Soluble VR1 Antagonist Using an Amorphous Solid Dispersion Approach: A Case Study. *Mol. Pharm.* **2008**, *5*, 981–993.
- (5) Sun, Y.; Zhu, L.; Wu, T.; Cai, T.; Gunn, E. M.; Yu, L. Stability of Amorphous Pharmaceutical Solids: Crystal Growth Mechanisms and Effect of Polymer Additives. *AAPS J.* **2012**, *14*, 380–388.
- (6) Schmelzer, J.; Pascova, R.; Möller, J.; Gutzow, I. Surface-induced devitrification of glasses: the influence of elastic strains. *J. Non-Cryst. Solids* **1993**, *162*, 26–39.
- (7) Tanaka, H. Possible resolution of the Kauzmann paradox in supercooled liquids. *Phys. Rev. E: Stat., Nonlinear, Soft Matter Phys.* **2003**, *68*, 011505.
- (8) Wu, T.; Sun, Y.; Li, N.; de Villiers, M. M.; Yu, L. Inhibiting Surface Crystallization of Amorphous Indomethacin by Nanocoating. *Langmuir* **2007**, 23, 5148–5153.
- (9) Wu, T.; Yu, L. Surface Crystallization of Indomethacin Below Tg. Pharm. Res. 2006, 23, 2350–2355.
- (10) Farrance, O. E.; Jones, R. A. L.; Hobbs, J. K. The observation of rapid surface growth during the crystallization of polyhydroxybutyrate. *Polymer* **2009**, *50*, 3730–3738.
- (11) Shi, Q.; Zhang, C.; Su, Y.; Zhang, J.; Zhou, D.; Cai, T. Acceleration of Crystal Growth of Amorphous Griseofulvin by Low-Concentration Poly(ethylene oxide): Aspects of Crystallization Kinetics and Molecular Mobility. *Mol. Pharm.* 2017, 14, 2262–2272.
- (12) Cai, T.; Zhu, L.; Yu, L. Crystallization of Organic Glasses: Effects of Polymer Additives on Bulk and Surface Crystal Growth in Amorphous Nifedipine. *Pharm. Res.* **2011**, *28*, 2458–2466.
- (13) Zhu, L.; Jona, J.; Nagapudi, K.; Wu, T. Fast Surface Crystallization of Amorphous Griseofulvin Below Tg. *Pharm. Res.* **2010**, 27, 1558–1567.
- (14) Zhang, S.-W.; Yu, L.; Huang, J.; Hussain, M. A.; Derdour, L.; Qian, F.; de Villiers, M. M. A Method to Evaluate the Effect of Contact with Excipients on the Surface Crystallization of Amorphous Drugs. AAPS PharmSciTech 2014, 15, 1516–1526.
- (15) Carlton, R. A. Polarized Light Microscopy. *Pharmaceutical Microscopy*; Springer, 2011; pp 7-64.
- (16) Moseson, D. E.; Mugheirbi, N. A.; Stewart, A. A.; Taylor, L. S. Nanometer-Scale Residual Crystals in a Hot Melt Extruded Amorphous Solid Dispersion: Characterization by Transmission Electron Microscopy. *Cryst. Growth Des.* **2018**, *18*, 7633–7640.
- (17) Bunaciu, A. A.; Udriştioiu, E. G.; Aboul-Enein, H. Y. X-Ray Diffraction: Instrumentation and Applications. *Crit. Rev. Anal. Chem.* **2015**, *45*, 289–299.
- (18) Chauhan, H.; Hui-Gu, C.; Atef, E. Correlating the Behavior of Polymers in Solution as Precipitation Inhibitor to its Amorphous Stabilization Ability in Solid Dispersions. *J. Pharm. Sci.* **2013**, *102*, 1924–1935.
- (19) Otaki, T.; Tanabe, Y.; Kojima, T.; Miura, M.; Ikeda, Y.; Koide, T.; Fukami, T. In situ monitoring of cocrystals in formulation development using low-frequency Raman spectroscopy. *Int. J. Pharm.* **2018**, *542*, 56–65.
- (20) Sinclair, W.; Leane, M.; Clarke, G.; Dennis, A.; Tobyn, M.; Timmins, P. Physical Stability and Recrystallization Kinetics of Amorphous Ibipinabant Drug Product by Fourier Transform Raman Spectroscopy. *J. Pharm. Sci.* **2011**, *100*, 4687–4699.
- (21) Bhatia, S.; Khanna, A.; Jain, R. K.; Hirdesh. Structure-property correlations in molybdenum trioxide thin films and nanoparticles. *Mater. Res. Express* **2019**, *6*, 086409.
- (22) Zhao, L.; Pinon, A. C.; Emsley, L.; Rossini, A. J. DNP-enhanced solid-state NMR spectroscopy of active pharmaceutical ingredients. *Magn. Reson. Chem.* **2018**, *56*, 583–609.
- (23) Thakral, N. K.; Mohapatra, S.; Stephenson, G. A.; Suryanarayanan, R. Compression-Induced Crystallization of Amorphous Indomethacin in Tablets: Characterization of Spatial Heterogeneity by Two-Dimensional X-ray Diffractometry. *Mol. Pharm.* 2015, 12, 253–263.

- (24) Bērziņš, K. r.; Suryanarayanan, R. Compression-Induced Crystallization in Sucrose-Polyvinylpyrrolidone Amorphous Solid Dispersions. *Cryst. Growth Des.* **2018**, *18*, 839–848.
- (25) Chowdhury, A. U.; Zhang, S.; Simpson, G. J. Powders Analysis by Second Harmonic Generation Microscopy. *Anal. Chem.* **2016**, *88*, 3853–3863.
- (26) Strachan, C. J.; Windbergs, M.; Offerhaus, H. L. Pharmaceutical applications of non-linear imaging. *Int. J. Pharm.* **2011**, *417*, 163–172.
- (27) Rawle, C. B.; Lee, C. J.; Strachan, C. J.; Payne, K.; Manson, P. J.; Rades, T. Towards characterization and identification of solid state pharmaceutical mixtures through second harmonic generation. *J. Pharm. Sci.* **2006**, *95*, 761–768.
- (28) Wanapun, D.; Kestur, U. S.; Taylor, L. S.; Simpson, G. J. Quantification of trace crystallinity in an organic powder by nonlinear optical imaging: Investigating the effects of mechanical grinding on crysallinity loss. Abstracts of Papers of the American Chemical Society, 2011; Vol. 241.
- (29) Podzemná, V.; Barták, J.; Málek, J. Crystal growth kinetics in GeS2 amorphous thin films. *J. Therm. Anal. Calorim.* **2014**, *118*, 775–781.
- (30) Sarkar, S.; Song, Z.; Griffin, S. R.; Takanti, N.; Vogt, A. D.; Ruggles, A.; Danzer, G. D.; Simpson, G. J. In Situ Crystal Growth Rate Distributions of Active Pharmaceutical Ingredients. *Mol. Pharm.* **2020**, *17*, 769–776.
- (31) Hancock, B. C.; Zografi, G. The Relationship Between the Glass Transition Temperature and the Water Content of Amorphous Pharmaceutical Solids. *Pharm. Res.* **1994**, *11*, 471–477.
- (32) Andronis, V.; Yoshioka, M.; Zografi, G. Effects of Sorbed Water on the Crystallization of Indomethacin from the Amorphous State. *J. Pharm. Sci.* **1997**, *86*, 346–351.
- (33) Katkov, I. I.; Levine, F. Prediction of the glass transition temperature of water solutions: comparison of different models. *Cryobiology* **2004**, *49*, 62–82.
- (34) Morris, K. R.; Griesser, U. J.; Eckhardt, C. J.; Stowell, J. G. Theoretical approaches to physical transformations of active pharmaceutical ingredients during manufacturing processes. *Adv. Drug Delivery Rev.* **2001**, 48, 91–114.
- (35) Sunagawa, I. Nucleation, Growth And Dissolution Of Crystals During Sedimentogenesis and Diagenesis. In *Developments in Sedimentology*; Wolf, K. H., Chilingarian, G. V., Eds.; Elsevier, 1994; Chapter 2, Vol. 51, pp 19–47.
- (36) Bauer, J.; Spanton, S.; Henry, R.; Quick, J.; Dziki, W.; Porter, W.; Morris, J. Ritonavir: An extraordinary example of conformational polymorphism. *Pharm. Res.* **2001**, *18*, 859–866.
- (37) Bates, S.; Zografi, G.; Engers, D.; Morris, K.; Crowley, K.; Newman, A. Analysis of Amorphous and Nanocrystalline Solids from Their X-Ray Diffraction Patterns. *Pharm. Res.* **2006**, 23, 2333–2349.
- (38) Findlay, W. P.; Bugay, D. E. Utilization of Fourier transform-Raman spectroscopy for the study of pharmaceutical crystal forms. *J. Pharm. Biomed. Anal.* **1998**, *16*, 921–930.
- (39) Song, Z.; Sarkar, S.; Vogt, A. D.; Danzer, G. D.; Smith, C. J.; Gualtieri, E. J.; Simpson, G. J. Kinetic Modeling of Accelerated Stability Testing Enabled by Second Harmonic Generation Microscopy (vol 90, pg 4406, 2018). *Anal. Chem.* **2018**, *90*, 13130.
- (40) Konno, H.; Taylor, L. S. Ability of Different Polymers to Inhibit the Crystallization of Amorphous Felodipine in the Presence of Moisture. *Pharm. Res.* **2008**, 25, 969–978.
- (41) Shamblin, S. L.; Zografi, G. The Effects of Absorbed Water on the Properties of Amorphous Mixtures Containing Sucrose. *Pharm. Res.* 1999, 16, 1119–1124.
- (42) Davies, M. J.; Seton, L.; Tiernan, N.; Murphy, M. F.; Gibbons, P. Towards crystal engineering via simulated pulmonary surfactant monolayers to optimise inhaled drug delivery. *Int. J. Pharm.* **2011**, 421, 1–11.
- (43) Garti, N.; Zour, H. The effect of surfactants on the crystallization and polymorphic transformation of glutamic acid. *J. Cryst. Growth* **1997**, *172*, 486–498.
- (44) Ben-Amotz, D. Understand Physical Chemistry; Self Published, 2019.

- (45) Zhang, F.; Meng, F.; Wang, Z. Y.; Na, W. Interpolymer complexation between copovidone and carbopol and its effect on drug release from matrix tablets. *Drug Dev. Ind. Pharm.* **2017**, *43*, 190–203.
- (46) Canselier, J. P. THE EFFECTS OF SURFACTANTS ON CRYSTALLIZATION PHENOMENA. J. Dispersion Sci. Technol. 1993, 14, 625–644.
- (47) Van den Mooter, G. The use of amorphous solid dispersions: A formulation strategy to overcome poor solubility and dissolution rate. *Drug Discovery Today: Technol.* **2012**, *9*, e79–e85.